Journal Name

ARTICLE TYPE

Cite this: DOI: 00.0000/xxxxxxxxxx

Selective hydrogenation of succinic acid to gamma-butyrolactone with PVP-capped CuPd catalysts

Son Dinh Le[a] and Shun Nishimura[a*]

Received Date
Accepted Date

DOI: 00.0000/xxxxxxxxxx

Selective hydrogenation of succinic acid (SA) is not an easy task especially toward γ-butyrolactone (GBL) which readily undergoes further hydrogenation. Herein, poly(*N*-vinyl-2-pyrrolidone)-capped CuPd catalysts have been studied for the production of highly selective GBL from SA. The optimal catalyst not only exhibited remarkable activity and stability but also preserved its efficiency even at a mild hydrogen pressure of 1 MPa and long recycling runs. The presence of PVP is proposed to play a key role in maintaining high selectivity of GBL in various conditions. Although a strong Cu–Pd interaction due to alloying formation is supposed to enhance the substrate adsorption, the GBL production could only be maximized if the CuPd alloy nanoparticles were enriched with Pd sites which are supposed to enhance the hydrogen activation.

1 Introduction

Heterogeneous metal nanoparticles (NPs) have been extensively investigated for hydrogenation of succinic acid (SA)[1,2]. The selection of metal was determined as a essential factor for the catalytic activity and selectivity to the target products. In general, group VIII metals such as Pd, Pt, and Rh are favorably used for hydrogenation reactions because H_2 can easily dissociated on the partially occupied d-orbitals of these metals[3]. Therefore, the development of heterogeneous catalysts for hydrogenation of SA has typically been studied on the synergy for enhancing the product yield and/or selectivity by combining a group VIII element with additional metals[1]. For example, Shao *et al.* reported that the monometallic Pd/C showed a low conversion of SA (48%) with high γ-butyrolactone (GBL) selectivity (94%)[4]. Depending on the amount of added Re in the Pd–Re bimetallic catalysts, the GBL yield can be improved (51–74%) which further converted to tetrahydrofuran (THF) as the reaction time prolonged. The structures and properties of metal NPs can be influenced by not only additional metal species but also the catalyst support[5]. For example, our recent study showed that the nature of support and metal–support interaction played an essential role in the construction of CuPd NPs, inducing tunable activity and selectivity for the SA hydrogenation[6].

Since the efficient hydrogenation of SA to GBL is generally difficult to accomplish due to excessive hydrogenation or hydrogenolysis reactions, the present study focuses on designing an effective catalyst which can minimize the rate of non-target reactions. Previously, several research focused on Pd-based catalysts for highly selective GBL had been reported[7–10]. For example, Zhang *et al.* indicated that beohmite nanosheets supported Pd catalysts can promote SA hydrogenation to afford GBL with excellent selectivities of 94–97%[9]. Even with very low metal loading from 0.1 to 1 wt% Pd, conversion of SA up to 97% can be achieved. In this research, however, elevated temperature (240 °C) and pressure (6 MPa) are required. A study from Yakabi *et al.* revealed that the SA hydrogenation can be proceeded at relatively mild conditions (140–170 °C and 1.5–3 MPa), affording >90% selectivity of GBL and <70% conversion of SA over the Pd/Al_2O_3 catalyst[10].

In fact, we previously reported that the hydrogenation of SA over the Cu/HAP monometallic catalysts can be used to afford GBL with excellent selectivity[11]. However, less than 20% conversion of SA was achieved, which can be attributed to the intrinsically low reactivity of Cu for hydrogen activation and dissociation[12]. In addition, our recent work showed that the TiO_2 supported CuPd bimetallic catalyst can enhance the catalyst activity for SA hydrogenation to GBL, affording a selectivity of 90% at 73% conversion of SA[6]. Nonetheless, it should be noted that the uses of high loading amounts of metals (10 wt%) in those cases posed several issues regarding metal leaching or agglomeration during the recycling tests resulted in decreases in the catalytic efficiency and product selectivity. The issues can be addressed by using a capping agent which is generally used in preparing and stabilizing well-defined metal NPs[13,14]. In addition, selectivity toward a certain product can be tuned in the presence of capping agent which is presumably due to the inhibition of substrate accessibility to a specific sites[15].

Given the potential of CuPd NPs for the hydrogenation of SA to GBL, as discussed in our previous work[6,11], the effect of a capping agent, i.e., poly(*N*-vinyl-2-pyrrolidone) (PVP) on the cat-

[a] *Graduate School of Advanced Science and Technology, Japan Advanced Institute of Science and Technology (JAIST), 1-1 Asahidai, Nomi, Ishikawa 923-1292, Japan*

† Electronic Supplementary Information (ESI) available. See DOI: 00.0000/00000000.

alytic performance of HAP supported CuPd NPs has been investigated in the present study. The catalysts were prepared using extremely low metal loadings (0.1 mmol) with the aim of enhancing the atom efficiency which is an important factor in industrial applications. It is worth noting that CuPd alloy catalysts can be prepared by different methods such as impregnation[16,17], chemical reduction[18,19], and other novel methods[20,21]. Herein, a polyol reduction method using 2-ethoxyethanol as a reducing agent is chosen because it requires simple metal sources as starting materials due to the water-comparable polarity of the polyols[22]. Furthermore, compared to other reducing agents used for CuPd alloy synthesis, such as sodium borohydride[19] and oleylamine[23], polyols are generally safer to handle and become reductive at high temperature[22]. A calcium orthophosphate of the apatite family named as HAP[24], is selected as the catalyst support. It is a nonporous material containing both weak acidic and basic sites, which may help to overcome mass transfer limitations and prevent side reactions[25]. Furthermore, HAP has high specific area and superior ion-exchanged capacity, and these natures lead to their high capacities for both metal immobilization on the surface and incorporation into its apatite framework[26,27].

The most promising catalyst was found by optimizing Cu:Pd molar ratio at 40:60 and stabilizing by PVP with the average molecular weight (M_w) of 40000 g mol^{-1}. The catalyst offered excellent activity and GBL selectivity even at very low hydrogen pressure (1 MPa) while maintaining its productivity up to 5 continuous runs. Extensive investigation on catalytic performance and characterization have been conducted and the roles of PVP and metal species are properly discussed.

2 Experimental

2.1 Materials

All the chemicals used in this study are listed in Table S1†.

2.2 Catalyst preparation

Poly(*N*-vinyl-2-pyrrolidone) (PVP)-capped Cu_xPd_y supported on hydroxyapatite (HAP), denoted as Cu_xPd_y−PVP/HAP, were prepared by polyol reduction method using PVP as a capping agent and 2-ethyoxyethanol as a reducing agent[28,29]. In a typical procedure, $Cu(OAc)_2 \cdot H_2O$ (x mmol) and $Pd(OAc)_2$ (y mmol) with $x+y = 0.1$ mmol are dispersed with PVP in 2-ethyoxyethanol (50 mL) and refluxed at 140 °C for 2 h. Subsequently, HAP (1.0 g) is added into the suspension which is further refluxed for another 1 h. The obtained solid is filtered and washed with deionized water (3 L) before being dried under a vacuum at room temperature.

2.3 Catalyst characterization

The crystal structures of catalysts were studied by using Powder X-ray diffraction (XRD) which was operated on a Rigaku Smart Lab X-ray diffractometer (Rigaku Co.) with a Cu Kα radiation (λ = 0.154 nm) at 40 kV and 30 mA. The database of the Joint Committee of Powder Diffraction Standard was used as references for analyzing observed diffraction patterns. The textural properties were examined using N_2-adsorption/desorption on a BELSORP-mini analyzer (MicrotracBEL Corp.). Surface areas and total pore volume are estimated based on the Brunauer-Emmett-Teller (BET) theory. The morphologies of catalysts were acquired by transmission electron microscopy (TEM) using H-7100 and H-7650 microscopes (Hitachi) operated at 100 kV. X-ray photoelectron spectra (XPS) were performed on an Axis-Ultra DLD spectrometer (Shimadzu Co. and Kratos Analytical Ltd.) with a monochromatic Al Kα (1486 eV) X-ray resource. The binding energies (BE) were calibrated using the C 1s spectrum of adventitious carbon contamination as an internal standard. XPS spectra were processed and analyzed by using the XPSPEAK4.1 software.

X-ray absorption fine structure (XAFS) spectra were recorded at the BL07 stations of the SAGA light source under the proposal nos. 1910092R and 2010015R. The storage ring was operated at 1.4 GeV where Si (220) single crystals was used to obtain monochromatic X-ray beams at Pd K-edge measurements. The catalysts were measured in fluorescence mode with an ion-chamber/SDD detector, while the references were measured in transmission modes with ion-chambers. Analyses of X-ray absorption near edge spectra (XANES) and extended X-ray absorption fine structure (EXAFS) were processed on the Athena and Artemis software of the Demeter suite version 0.9.26.

2.4 Catalyst evaluation

A solution containing 1,4-dioxane (10 mL), SA (0.1 g) and the reduced catalyst (0.1 g) was mixed in an inner glass vessel and placed in a stainless-steels autoclave reactor (Taiatsu Technol., Japan). Before reaction the reactor was purged from the remaining air, followed by pressurizing to a certain pressure by pure H_2 (99.999%) at room temperature. The reactor was then placed into an aluminum block heated prior at 200 °C under vigorous stirring. After reaction the reaction mixture was centrifugated and the products were analyzed by gas chromatography (GC, Shimadzu GC-2014) with a polar column (DB-FFAP, Agilent). The GC column program was increased from initial temperature of 50 °C (keep for 2 min) to 240 °C (keep for 5 min) at a rate of 20 °C min^{-1}. Whereas the temperatures at injection port and the detector were 250 °C and 280 °C, respectively. The SA conversion was analyzed by high-performance liquid chromatography (HPLC, Water 2414) equipped with a refractive index detector. An aqueous solution of H_2SO_4 (10 mM) was used as an eluent, which was pumped at a flow rate of 0.5 mL min^{-1} through an Aminex HPX-87H column (Bio-Rad) operated at 50 °C.

3 Results and discussion

3.1 Catalytic performance

3.1.1 Influence of capping agents on the performances of HAP supported CuPd catalysts

In an attempt to search for a suitable capping agent, common polymers including PVP, PVA, and starch were used to prepare HAP supported CuPd catalysts. The prepared catalysts were employed for the hydrogenation of SA and the results are shown in Figure S1†. PVP, which is a weakly adsorbing stabilizer, was emerged as a potential capping agent since the resulting catalyst can accelerate the SA hydrogenation to GBL with excellent yield. Whereas the catalyst prepared without capping agent or

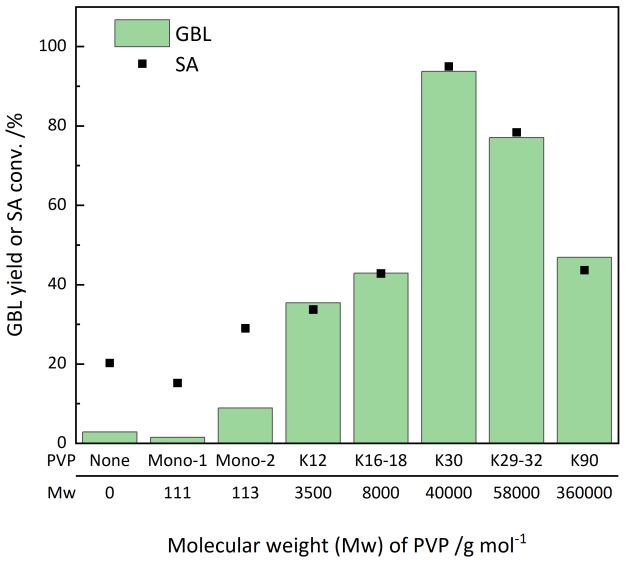

Fig. 1 Effect of molecular weight of PVP on the hydrogenation of SA over HAP supported CuPd catalysts. Reaction conditions: SA (0.1 g), $Cu_{40}Pd_{60}$−PVP/HAP (0.1 g), 1,4-dioxane (10 mL), temperature (200 °C), H_2 pressure (8 MPa), reaction time (48 h). Note: Mono-1 (1-vinyl-2-pyrrolidone), Mono-2 (1-ethyl-2-pyrrolidone).

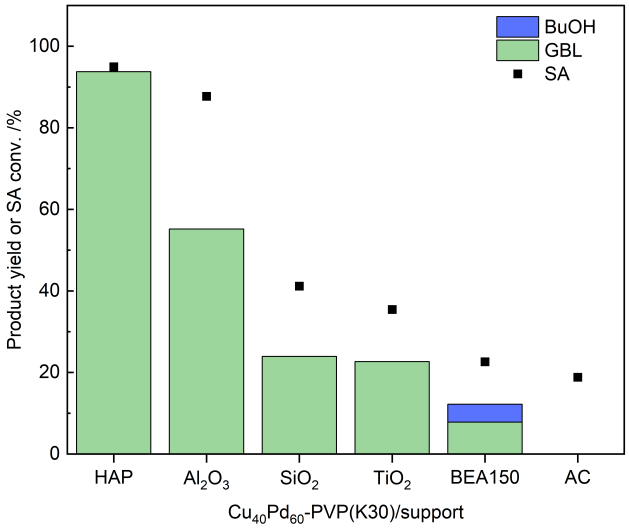

Fig. 2 Influence of support on the activity of CuPd catalyst. Reaction conditions: SA (0.1 g), catalyst (0.1 g), 1,4-dioxane (10 mL), reaction temperature (200 °C), H_2 pressure (8 MPa), reaction time (48 h). 1-butanol: BuOH

with other stabilizing polymers exhibited extremely low activities, which probably can be contributed to the metal agglomeration during the catalyst preparation.

The effect of molecular weight (Mw) of PVP on the catalyst activity and stability of various metals including Cu and Pd NPs has been widely reported[30–33]. However, the influence of the chain length of stabilizing polymer on the CuPd NPs remains elusive. Therefore, herein, the catalytic activity of CuPd NPs as a function of PVP Mw for the SA hydrogenation has been examined (Figure 1). It is observed that the increase in PVP chain length resulted in better catalytic performance. This enhancement in the catalytic activity might be attributed to the positive role of PVP in the formation of well-defined CuPd NPs. As a result, a maximum yield of GBL at 95% yield and 99% selectivity was obtained over the CuPd NPs capped with PVP K30 (Mw = 40000). Further increasing the chain length of PVP, however, caused adverse effects on the activity since the GBL started decreasing and lost 50% in the case of CuPd NPs capped with PVP K90 (Mw = 360000). The negative impact of long-chain polymers can be explained by the blocking of active sites that limits the accessibility of the reactants[22].

3.1.2 Effect of Support on the Catalytic Performance of PVP(K30) capped CuPd NPs

Various common supports have been used to investigate their impacts on the catalytic performance of the PVP capped CuPd NPs. Figure 2 indicates that HAP is the most suitable support for achieving the superior catalytic performance (96% of SA conversion with 95% of GBL yield). It is worth noting that in our previous reports the product selectivity over CuPd catalyst without capping agent was varied depending on the support[6,11]. However, here with the presence of PVP, GBL was obtained as the main product regardless of the catalyst support, implying the weaker influence of support to the capping agent. Nevertheless, in terms of catalytic activity and GBL selectivity, HAP represents the best catalyst support due to its unique properties, i.e., coexistence of weakly acidic and basic sites and ion exchangeability[25–27], as discussed in the previous section. Whereas the lower activity and selectivity in other catalyst supports may be ascribed to their lower metal dispersions and/or the presence of strong acidic sites which promotes side reactions. Note that the lower carbon balance in these cases can be caused by the formation of gaseous products via over-reduction, dehydration, or cracking reactions[34].

3.1.3 Effect of Metal Ratio on the Catalytic Activity

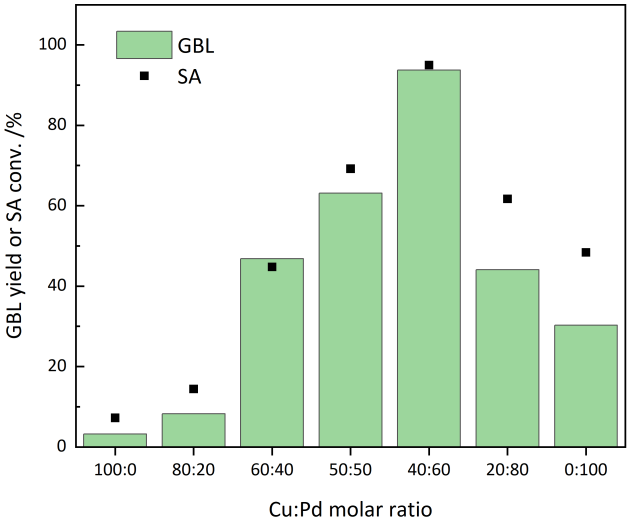

Fig. 3 Influences of metal ratio on the activities of Cu_xPd_y−PVP/HAP catalysts. Reaction conditions: SA (0.1 g), catalyst (0.1 g), 1,4-dioxane (10 mL), temperature (200 °C), H_2 pressure (8 MPa), reaction time (48 h).

It is noted that the non-capped CuPd NPs supported on HAP catalyzed SA hydrogenation toward butyric acid (BA) or 1,4-butanediol (BDO) with high selectivities, as reported in our previous research[11]. However, by using PVP as capping agent, the catalytic behavior fundamentally changed since only GBL was observed. As also revealed in the previous work that the Cu monometallic catalysts yielded GBL as a major product, the high selectivity of GBL over PVP capped CuPd NPs suggests a partial inhibition of Pd and an enhanced role of Cu. Therefore, it is desirable to investigate the influence of metal ratio on the catalytic activity of the Cu_xPd_y−PVP(K30)/HAP. Figure 3 confirms the low activity of monometallic Cu as less than 5% yield of GBL can be observed. Upon addition of Pd, the formation of GBL increased and reached its peak at a yield of 94% over the $Cu_{40}Pd_{60}$−PVP/HAP. Further increasing Pd contents led to the decreases in catalytic activity and selectivity since GBL yield dropped dramatically to 30% over the monometallic Pd catalyst. These results first indicate the importance of bimetallic catalysts for the enhancement in catalytic activity and GBL selectivity, compared to the monometallic ones. Second, the high selectivities of GBL point out the significance of PVP in controlling the catalytic selectivity by preventing both Cu and Pd sites from further reduction to BDO and hydrolysis to BA, respectively.

The reactions over catalysts with higher metal loading were performed as indicated in Figure S2†. It is observed that PVP can maintain its impact even at relatively high metal loading. Since the $Cu_{40}Pd_{60}$−PVP/HAP, which contains the greater fraction of Pd, was used, BA with small quantities can be observed at higher metal loadings ($\leq$ 0.5 mmol). However, a small fraction of BDO was only formed over the $Cu_{40}Pd_{60}$−PVP/HAP with a significantly high metal loading of 1 mmol. This result can be attributed to the low reactivity of Cu species in comparison with the precious metal Pd. A doubled amount of catalyst can yield BDO with greater selectivity, however, GBL is still maintained as the dominant product. It is also noted that when metal loading was greatly increased, Cu seemed to take over the role of Pd since no BA was detected. This might suggest changes in the CuPd structures or morphologies.

3.1.4 Influences of reaction conditions on the catalytic performance

The hydrogenation of SA is a complex reaction consisting of several pathways towards different products, which strongly depends on the choice of reaction conditions such as temperature and H_2 pressure. A review from Delhomme *et al.* summarized that temperatures above 150 °C are generally required to obtain optimal performance of SA hydrogenation[1]. On the other hand, according to the results from our previous work[11], the GBL formation was favorable at a lower temperature than 200 °C. Thus, the reaction temperatures in a range of 150–200 °C were used to carry out the reaction over the present catalyst. The effect of temperature on the overall reaction performance are demonstrated in Figure 4A. The results, however, show that at the lower reaction temperature, the GBL yield reduced significantly to just above 30% and less than 5% at 180 °C and 150 °C, respectively. This might be ascribed to the small amount of metal loading and the negative impact of PVP on the active site, which requires greater activation energy, compared to that over the CuPd catalysts without capping agent[11].

The influence of H_2 pressure for the current reaction was examined and the results are shown in Figure 4B. In comparison with the productions of BDO and THF which typically require high pressures of H_2 due to the needs of 8 hydrogen atoms for 2-step hydrogenation from SA, the formation of GBL require only a half of the hydrogen consumption. As a result, lower H_2 pressure might be sufficient for the GBL production. A previous research reported that 3 MPa of hydrogen can catalyze SA hydrogenation to afford GBL with greater than 90% selectivity and less than 70% SA conversion[10]. The present work has recorded even milder hydrogen pressure, i.e, 2 MPa, which efficiently converted SA to GBL with 95% selectivity at 84% SA conversion. The excellent selectivity can be maintained at a lower pressure of 1 MPa, however, the SA conversion slightly decreased to about 70%. An attempt to further reduce the H_2 pressure to as low as the atmospheric pressure has been made but was unsuccessful since no GBL can be detected. There might be two important factors, i.e, H_2 dissociation and diffusion, that attribute to the efficiency of catalytic performance at relatively low hydrogen pressure. For example, the presence of PVP first can help to enhance the metal dispersion which subsequently increases the hydrogen adsorption and diffusion in the metal surface. Second, as reported in both practical[35] and theoretical[36] methods, PVP can also serve as an electron donor which increases the electron density around the Pd atoms, facilitating the H_2 dissociation step.

3.2 Catalyst Characterization and Structure–Activity Relationship

3.2.1 Influence of metal ratio on the sizes of CuPd NPs

As indicated in Figure 5, the CuPd NPs show small sizes ranging from 1.9 to 3.7 nm. NPs with larger diameters of 3.8 nm and 4.7 nm can be observed in the monometallic catalysts Pd and Cu, respectively. The variation in sizes among these samples suggests that NP size depends mainly on the nature of metals and the ratio between them. To some extent, PVP can enhance the immobilization efficiency due to the binding affinity to the metal surface[37], which resulted in well-dispersed NPs in the prepared catalysts. However, it seems that at the early steps of polyol process, PVP was unable to control the particle size of the catalyst with high Cu contents. Indeed, in the cases of Cu_{80} and Cu_{100} catalysts, non-uniform particles, i.e., broad size distributions, were observed. Nonetheless, in the later steps of particle growing when particles grew to a certain size, the presence of PVP helped to minimize the metal agglomeration. For examples, although large particles can be observed in the Cu_{80} and Cu_{100}, the average sizes are less than 5 nm in average, compared to that of the catalyst without PVP (Figure S3†).

The XRD patterns of the catalysts and references were plotted in Figure S4†. It is observed that the diffraction lines of all the samples resemble the pattern of HAP. No diffraction peaks corresponding to the Cu or Pd metal references can be detected even in the cases of monometallic catalysts. These results can be con-

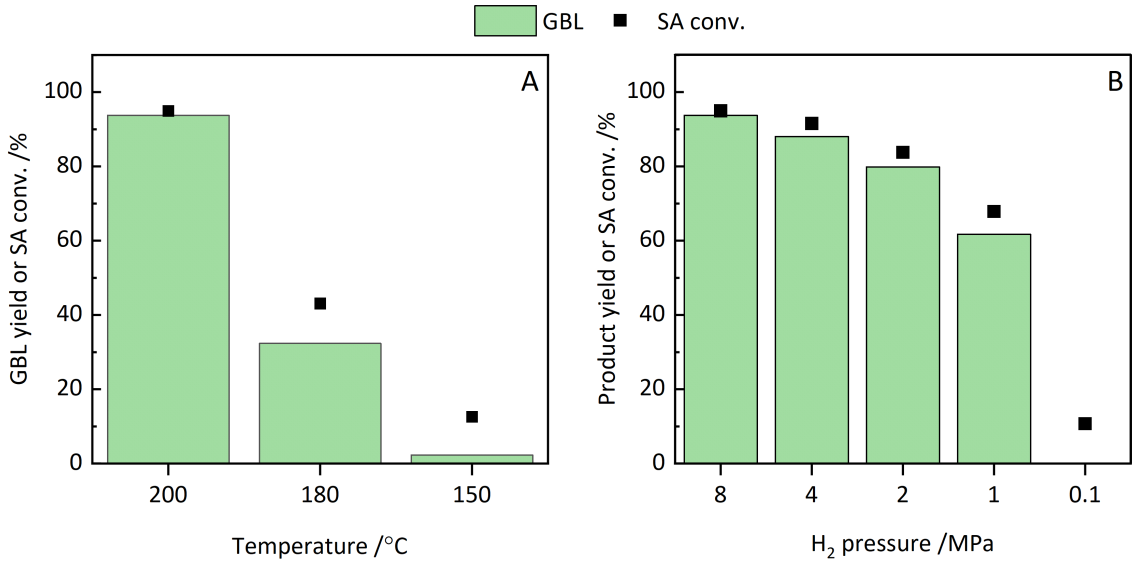

Fig. 4 (A) Effects of temperature and (B) H_2 pressure on the SA hydrogenation over the $Cu_{40}Pd_{60}$−PVP/HAP catalyst. Reaction conditions: SA (0.1 g), catalyst (0.1 g), 1,4-dioxane (10 mL), H_2 pressure (8 MPa) for (A) temperature (200 °C) for (B), reaction time (48 h).

tributed to the low amount of metal loaded and the stronger XRD intensity (crystallinity) of the HAP support. In order to clarify the interaction between Cu and Pd, the unsupported catalyst was prepared and measured by XRD. Figure S5† shows that the lattice parameter (3.74 Å) for the $Cu_{40}Pd_{60}$−PVP/HAP catalyst lies between the values for Pd (3.96 Å) and Cu (3.62 Å) references, indicating the alloying formation between these two metals.

N_2 adsorption/desorption results are shown in Figure S6†, which is also consistence with the results obtained by XRD. Accordingly, a type II adsorption/desorption isotherm, which is characteristic nonporous materials, is observed in both the bare support and the $Cu_{40}Pd_{60}$−PVP/HAP catalyst. In addition, there is no significant difference in the total volume (V_p) and surface area (S_{BET}) between the support and catalyst, indicating that the HAP structure was preserved after metal loading and small amount of metal with well-dispersed NPs were deposited on the surface of the support.

3.2.2 Electronic structures and metal interactions

XPS was performed to determine the surface composition, electronic properties, and the interaction between Cu and Pd. Figure 6A demonstrates the spectra at Cu 2p region where Cu $2p_{3/2}$ and Cu $2p_{1/2}$ components can be observed at 933 eV and 953 eV, respectively, due to spin-orbit splitting. The deconvoluted peak at Cu $2p_{3/2}$ indicates the presence of Cu^0 (∼933 eV) as a dominant phase. While in some cases, Cu^{2+} (∼935 eV) can be involved in the fits due to partial oxidations during the XPS sampling. Similarly, XPS spectra at 3*d* region can be characterized by Pd $3d_{5/2}$ and Pd $3d_{3/2}$ components at about 335 eV and 340 eV, respectively (Figure 6B). The XPS peak at Pd $3d_{5/2}$ region can be fitted with Pd^0 and Pd^{2+} components at about 335 eV and 336–337 eV, respectively. It is noted that the best fit for $Cu_{40}Pd_{60}$−PVP/HAP catalyst showed the surface exposure of only metallic Pd species, indicating its strong resistance to oxidation. Detailed information about the exposed surfaces and their binding energies of the Cu_yPd_y−PVP/HAP catalysts can be found in Table S3†. Accordingly, BE shifts of 0–0.4 eV to lower values can be observed in the Cu^0 $2p_{3/2}$ of the bimetallic catalysts with respect to that of the monometallic Cu catalyst. Whereas positive BE shifts of 0.3–0.5 eV were estimated at Pd^0 $3d_{5/2}$ compared to that of the monometallic Pd catalyst. These shifts suggest charge transfers from Pd to Cu resulting from strong interaction, i.e., alloying, between these two metals[38,39]. It is worth mentioning that the direction of charge transfer in this case is opposite to what was observed in the HAP supported catalysts without capping agent in our previous study[11]. This can further emphasize the strong impacts of PVP to the net-charge flow between Cu and Pd and then to the electronic structure of the whole catalyst system.

Figure 7A describes XANES spectra of Cu_xPd_y−PVP/HAP catalyst at Pd K-edge. In all samples, white lines are not observed indicating the prevalence of Pd in the metallic state. However, the first neighboring peaks in these catalysts are lower in intensity compared to that of the Pd foil, suggesting the existences of Pd^{2+} components. Linear combination fitting (LCF) was then performed to qualitatively determine the oxidation states of Pd (Figure 7B). The fraction of Pd^{2+} in the $Cu_{20}Pd_{80}$ catalyst is substantially larger than that of the others. These results can be rationalized by referring to the NP size of this sample. Particularly, as revealed by TEM (Figure 5), the constructed NPs in this sample is extremely small compared to others resulted in the enhancements of specific surface area and metal–oxygen coordination. Therefore, the lowest fraction of Pd^{2+} in the $Cu_{40}Pd_{60}$ catalyst can be attributed to not only the stability of Pd–Cu bonding but also the larger NPs which are hard to be oxidized completely when exposing to the air after reduction. Despite the fact that more Pd–Cu bonds can be formed upon addition of Cu, the dominance of Cu contents in the bimetallic catalysts can result in larger Pd^{2+} components due to the migration of oxygen from CuO–Pd interface to Pd[40]. As a result, the metallic contents of Pd decreased in the $Cu_{60}Pd_{40}$ and $Cu_{80}Pd_{20}$ catalysts.

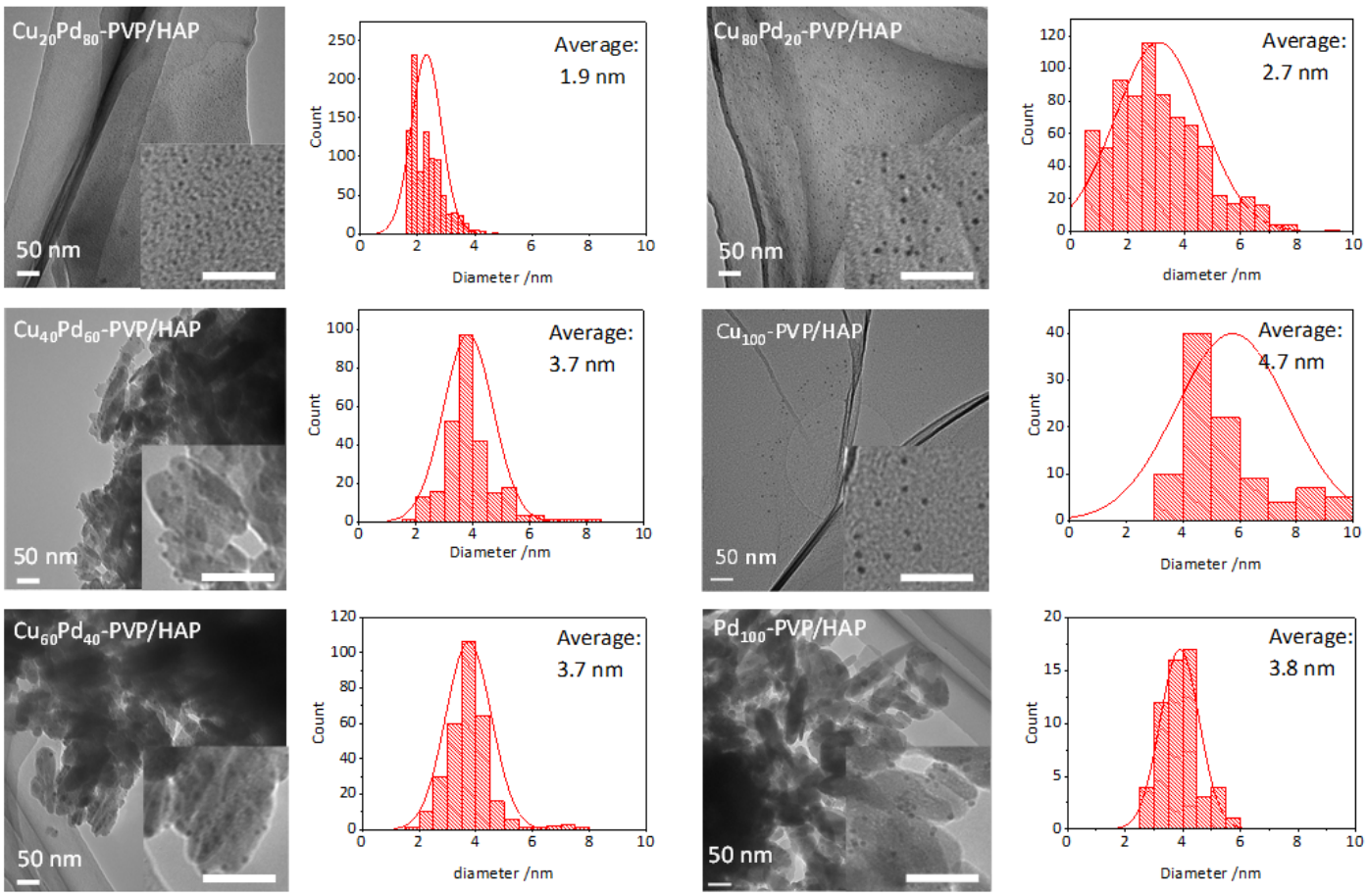

Fig. 5 Effect of metal ratio on the sizes of CuPd NPs as revealed by TEM. Corresponding zoomed insets are provided at the bottom right corners for better visualization.

Table 1 Fitting results at Pd K-edge for Cu_xPd_y−PVP/HAP

Sample	CN_{Pd-Pd}	CN_{Pd-Cu}	R_{Pd-Pd} (Å)	R_{Pd-Cu} (Å)
Pd foil	12	-	2.74	-
Pd_{100}	6.1 ± 0.9	-	2.74	-
Pd_{80}	3.2 ± 0.4	-	2.72	-
Pd_{60}	4.7 ± 0.6	1.4 ± 0.5	2.71	2.66
Pd_{40}	3.0 ± 0.2	2.1 ± 0.2	2.68	2.59
Pd_{20}	2.5 ± 0.7	2.2 ± 0.7	2.69	2.61

The k^3-weighted EXAFS spectra indicate slight decreases in the $\chi(k)$ signal amplitude for the oscillation peak at about 2.5 Å upon increasing of Cu contents (Figure S7†). These peaks are broadened and shifted to higher k values compared to the Pd reference. This observation indicates the decreases in the average Pd–Pd CNs which could be substituted by Pd–Cu and/or Pd–O coordinations in the bimetallic catalysts.

The Fourier transform (FT) EXAFS spectra of raw and fitted data at Pd K-edge for the Cu_xPd_y−PVP/HAP catalysts are visually demonstrated in Figure 8. While the details on the coordination number (CN) and atomic distance (R) are listed in Table 1. The peaks corresponding to Pd–Pd appeared at about 2.5 Å, whereas adjacent peaks at about 2.2 Å representing Pd–Cu bonding can be observed in the bimetallic catalysts. Except for the $Cu_{20}Pd_{80}$−PVP/HAP which contains a small amount of Cu, Cu can be involved in the fits of other bimetallic catalysts. The fitting results indicate that CN of Pd–Cu increased with the addition of Cu content, which confirms the strong interaction between Cu and Pd as a result of alloying formation. CNs revealed by EXAFS also provide useful information pertaining to the compositional of bimetallic NPs[41]. In the three samples (Pd_{20-60}) whose Pd–M (M = Pd, Cu) can be estimated, it was observed that $\frac{CN_{Pd-Pd}}{CN_{Pd-Cu}} > \frac{x_{Pd}}{x_{Cu}}$, where the right-hand side represents the theoretical ratio of bulk concentration of Pd and Cu in the samples. This result suggests that either the intra-particle or inter-particle segregation is present in these alloy NPs[42].

Given the superior catalytic performances of bimetallic catalysts compared to the monometallic ones (Figure 3A), CuPd alloying are proposed to be a prerequisite factor. In particular, the charge transfers from Pd to Cu might lead to positive Pd sites which enhanced the adsorption of SA. However, it seems that it is not sufficient to obtain an excellent yield of GBL because, for example, greater alloying degrees in Pd_{40} and Pd_{20} cannot help them in enhancing the GBL yield. Therefore, there must be another factor that is responsible for this. It is worth noting that the Pd–Pd ensembles remained as a comparable phase to the Pd–Cu. The decreases of Pd–Pd CN from 4.7 to 2.5 are found to be aligned with the reduction of GBL in the bimetallic catalysts.

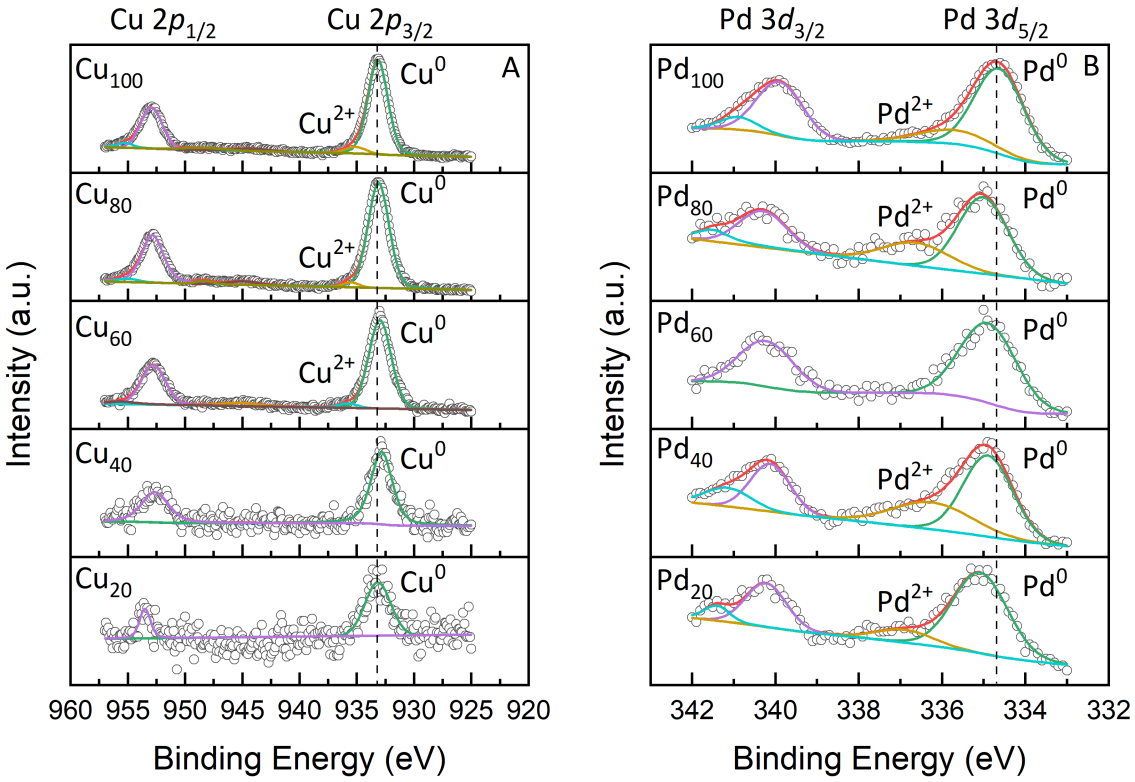

Fig. 6 Deconvoluted XPS spectra of Cu_xPd_y−PVP/HAP catalysts at (A) Cu 2*p* and (B) Pd 3*d* regions

According to Yang *et al.*, the adsorption energy of hydrogen on the $Pd_1Cu_3(111)$ is lower than on the Pd(111)[43], which can be attributed to the unsuitable geometries due to larger Pd–Pd distance[44]. In other words, the efficiencies of hydrogen adsorption and dissociation might be lower on the CuPd alloying sites than on the Pd sites, which is possibly responsible for the decreases in catalytic activity. Therefore, it is suitable to propose that in terms of the catalytic activity, Pd rich CuPd alloying NPs are necessary and sufficient conditions for the optimum efficiency of GBL production.

3.3 Catalyst stability

To evaluate the catalyst stability, the used catalyst was washed with 1,4-dioxane (4 × 5 mL) and dried in a vacuum before using for the subsequent run. In terms of GBL yield, the $Cu_{40}Pd_{60}$−PVP/HAP shows excellent reusability for up to 5 consecutive runs (Figure 9A). However, the GBL selectivity gradually decreased during the recycling tests where just about 79% could be obtained in the fifth run. To compare the structure with the fresh catalyst, the used catalyst was then characterized by XAFS. The FT EXAFS of raw and fitting data at Pd K-edge are shown in Figure 9B and Table S2, while XANES and k^3-weighted EXAFS spectra are presented in Figure S8†. According to the fitting results in R space, the Pd–Pd CN of the used catalyst is 2.7 ± 0.6, which is lower than that of the fresh one (4.7 ± 0.6). It is noted that CN of Pd–Cu increased after recycling runs, particularly from 1.4 ± 0.5 in the fresh catalyst to 2.2 ± 0.5 in the used catalyst. This can be contributed to the decrease in the Cu–O coordination due to the reduction during the reaction. As a result, more Cu is available to be coordinated with Pd. In addition, as shown in Figure S8A†, a stronger white line can be observed in the fresh catalyst, which indicates a higher valance state of Pd compared to that of the used catalyst. The lower valence state of Pd in the used catalyst can be attributed to the *in-situ* reduction by hydrogen during the reaction. These results, in combination with the previous discussion, indicates that Pd–Pd coordination is crucial not only for optimizing the GBL yield but also its selectivity. Nevertheless, considering the fact that the $Cu_{20}Pd_{80}$ and $Cu_{60}Pd_{40}$ catalysts have a similar Pd–Pd CN but the GBL selectivity over the latter is higher, it is concluded that both Pd–Pd and Pd–Cu is necessary for efficient production of GBL.

3.4 Flow reactor activity tests

The reaction under low hydrogen pressure that is available in the batch reaction opens up a possibility to carry out the SA hydrogenation using a flow reaction system (Figure S9†). As presented in Figure 10, the GBL yield of 17–18% can be maintained for 12 h at 0.5 MPa. According to the initial result herein along with the results obtained in batch reactor, it is believed that the GBL yield can be enhanced by increasing hydrogen pressure and optimizing other reaction parameters.

4 Conclusion

In conclusion, a highly efficient PVP-capped CuPd catalyst constructed on HAP was discovered for selective hydrogenation of SA to GBL. The capping agent PVP played an important role in con-

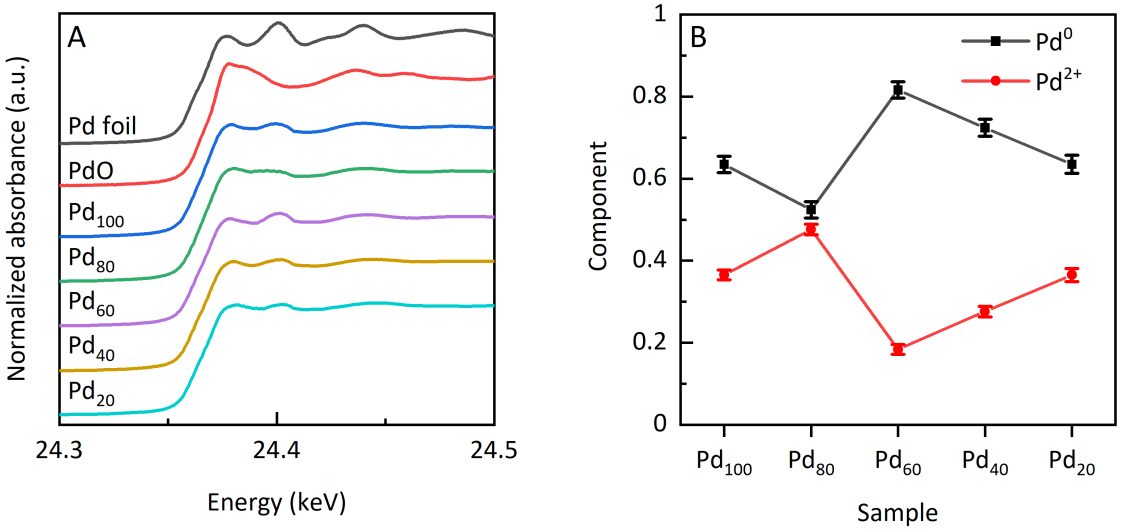

Fig. 7 (A) XANES spectra and (B) LCF results for Cu_xPd_y−PVP/HAP at Pd K-edge

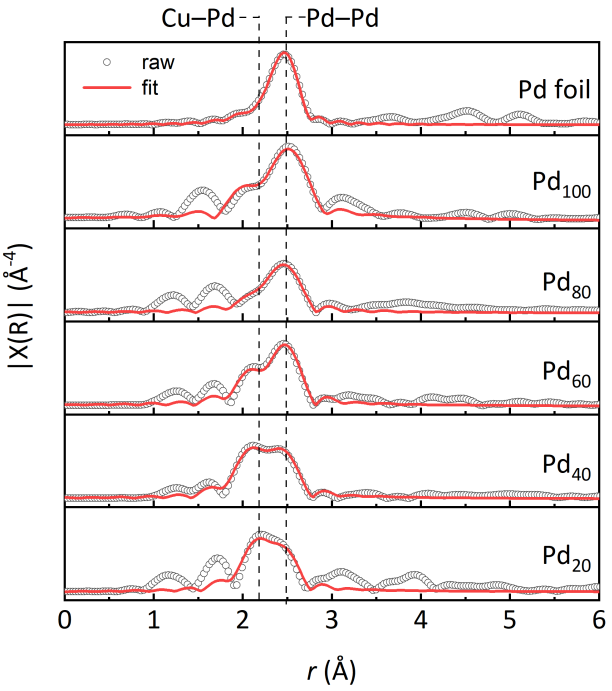

Fig. 8 FT EXAFS spectra of Cu_xPd_y−PVP/HAP at Pd K-edge

trolling the GBL selectivity by preventing further hydrogenation or other side reactions. While low activities could be observed in the monometallic catalysts, the reaction over the optimized $Cu_{40}Pd_{60}$−PVP/HAP catalyst exhibited remarkable enhancement in the production of GBL. XPS revealed a strong interaction between Cu and Pd leading to unique properties of the bimetallic catalysts. XAFS suggested the metallic Pd that exists close to the Cu–Pd alloying phase as a prominent factor to afford remarkable activity in the optimized catalyst. The catalyst was able to perform at low hydrogen pressure from 1 MPa while maintaining high selectivity of GBL (>90%). Also, together with the remarkable reusability and possibility for flow reaction, the present catalyst is potentially available for hydrogenation of not only SA but also other oxygen-rich biomass resources from laboratory to industrial scale.

Author Contributions

Son Dinh Le: Conceptualization, Data curation, Investigation, Writing-Original draft, Writing-Review & Editing. **Shun Nishimura:** Resources, Methodology, Writing-Review & Editing, Supervision.

Conflicts of interest

There are no conflicts to declare.

Acknowledgements

This study was supported by the JSPS KAKENHI for Young Scientists (A) (grant No. 17H04966), Japan. S.D.L greatly acknowledges the financial support from the Doctoral Research Fellowship (DRF) scholarship at JAIST.

References

1 C. Delhomme, D. Weuster-Botz and F. E. Kühn, *Green chemistry*, 2009, **11**, 13–26.

2 A. Mazière, P. Prinsen, A. García, R. Luque and C. Len, *Biofuels, Bioproducts and Biorefining*, 2017, **11**, 908–931.

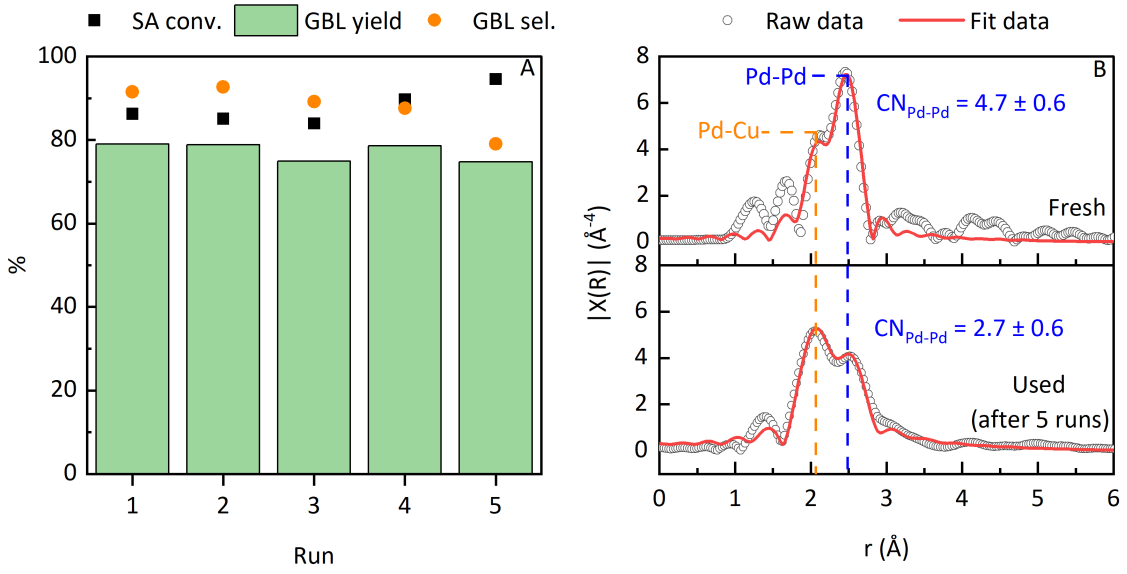

Fig. 9 (A) Reusability tests for the $Cu_{40}Pd_{60}$−PVP/HAP catalyst. Reaction condititons: SA (0.1 g), catalyst (0.1 g), 1,4-dioxane (10 mL), H_2 pressure (8 MPa), temperature (200 °C), reaction time (24 h). (B) FT EXAFS spectra at Pd K-edge of the fresh and used catalysts.

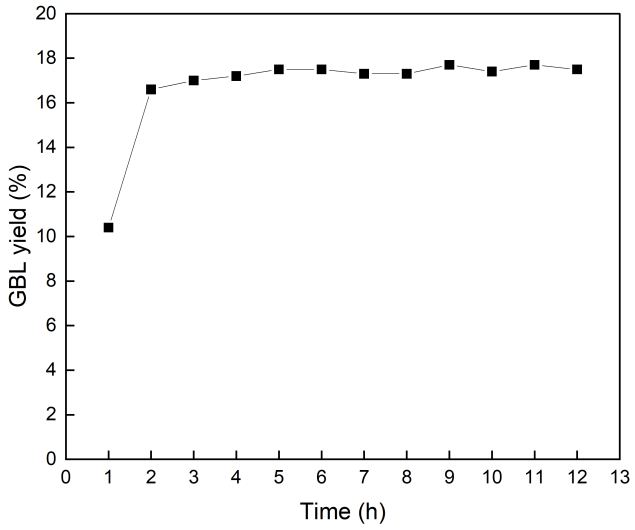

Fig. 10 GBL production over flow reactor system. Reaction conditions: SA (0.05 M), catalyst bed (0.5 g), liquid flow rate (0.3 mL min^{-1}), H_2 flow rate (10 mL min^{-1}), H_2 pressure (0.5 MPa), temperature (200 °C).

3 L. Zhang, M. Zhou, A. Wang and T. Zhang, *Chemical reviews*, 2019, **120**, 683–733.

4 Z. Shao, C. Li, X. Di, Z. Xiao and C. Liang, *Industrial & Engineering Chemistry Research*, 2014, **53**, 9638–9645.

5 L. Liu and A. Corma, *Chemical reviews*, 2018, **118**, 4981–5079.

6 S. D. Le and S. Nishimura, *Applied Catalysis B: Environmental*, 2021, **282**, 119619.

7 C. You, C. Zhang, L. Chen and Z. Qi, *Applied Organometallic Chemistry*, 2015, **29**, 653–660.

8 U. G. Hong, S. Hwang, J. G. Seo, J. Lee and I. K. Song, *Journal of Industrial and Engineering Chemistry*, 2011, **17**, 316–320.

9 C. Zhang, L. Chen, H. Cheng, X. Zhu and Z. Qi, *Catalysis Today*, 2016, **276**, 55–61.

10 K. Yakabi, A. Jones, A. Buchard, A. Roldan and C. Hammond, *ACS Sustainable Chemistry & Engineering*, 2018, **6**, 16341–16351.

11 S. D. Le and S. Nishimura, *ACS Sustainable Chemistry & Engineering*, 2019, **7**, 18483–18492.

12 K. Cao, G. Füchsel, A. W. Kleyn and L. B. Juurlink, *Physical Chemistry Chemical Physics*, 2018, **20**, 22477–22488.

13 A. R. Tao, S. Habas and P. Yang, *Small*, 2008, **4**, 310–325.

14 A. Heuer-Jungemann, N. Feliu, I. Bakaimi, M. Hamaly, A. Alkilany, I. Chakraborty, A. Masood, M. F. Casula, A. Kostopoulou, E. Oh *et al.*, *Chemical reviews*, 2019, **119**, 4819–4880.

15 P. Liu, R. Qin, G. Fu and N. Zheng, *Journal of the American Chemical Society*, 2017, **139**, 2122–2131.

16 A. J. McCue, C. J. McRitchie, A. M. Shepherd and J. A. Anderson, *Journal of catalysis*, 2014, **319**, 127–135.

17 K. A. Goulas, S. Sreekumar, Y. Song, P. Kharidehal, G. Gunbas, P. J. Dietrich, G. R. Johnson, Y. Wang, A. M. Grippo, L. C. Grabow *et al.*, *Journal of the American Chemical Society*, 2016, **138**, 6805–6812.

18 M. Yamauchi, R. Abe, T. Tsukuda, K. Kato and M. Takata, *Journal of the American Chemical Society*, 2011, **133**, 1150–1152.

19 V. S. Marakatti, S. C. Sarma, B. Joseph, D. Banerjee and S. C. Peter, *ACS applied materials & interfaces*, 2017, **9**, 3602–3615.

20 L. Di, W. Xu, Z. Zhan and X. Zhang, *RSC Advances*, 2015, **5**, 71854–71858.

21 D. Chen, P. Sun, H. Liu and J. Yang, *Journal of Materials Chemistry A*, 2017, **5**, 4421–4429.

22 L. M. Rossi, J. L. Fiorio, M. A. Garcia and C. P. Ferraz, *Dalton Transactions*, 2018, **47**, 5889–5915.

23 Y. Mun, S. Lee, A. Cho, S. Kim, J. W. Han and J. Lee, *Applied Catalysis B: Environmental*, 2019, **246**, 82–88.

24 A. Fihri, C. Len, R. S. Varma and A. Solhy, *Coordination Chem-*

istry Reviews, 2017, **347**, 48–76.

25 G. Xu, Y. Zhang, Y. Fu and Q. Guo, *ACS Catalysis*, 2017, **7**, 1158–1169.

26 H. Sun, F.-Z. Su, J. Ni, Y. Cao, H.-Y. He and K.-N. Fan, *Angewandte Chemie International Edition*, 2009, **48**, 4390–4393.

27 H. Tounsi, S. Djemal, C. Petitto and G. Delahay, *Applied Catalysis B: Environmental*, 2011, **107**, 158–163.

28 K. A. Guy, H. Xu, J. C. Yang, C. J. Werth and J. R. Shapley, *The Journal of Physical Chemistry C*, 2009, **113**, 8177–8185.

29 S. Nishimura, N. Yoshida and K. Ebitani, *MRS Online Proceedings Library (OPL)*, 2015, **1760**, mrsf14–1760–yy05–32.

30 M. Tsuji, Y. Nishizawa, K. Matsumoto, M. Kubokawa, N. Miyamae and T. Tsuji, *Materials letters*, 2006, **60**, 834–838.

31 S. Haesuwannakij, T. Kimura, Y. Furutani, K. Okumura, K. Kokubo, T. Sakata, H. Yasuda, Y. Yakiyama and H. Sakurai, *Scientific reports*, 2017, **7**, 1–8.

32 L. S. B. Upadhyay and N. Kumar, *Inorganic and Nano-Metal Chemistry*, 2017, **47**, 1436–1440.

33 G.-H. Han, S.-H. Lee, M.-g. Seo and K.-Y. Lee, *RSC Advances*, 2020, **10**, 19952–19960.

34 D. R. Vardon, A. E. Settle, V. Vorotnikov, M. J. Menart, T. R. Eaton, K. A. Unocic, K. X. Steirer, K. N. Wood, N. S. Cleveland, K. E. Moyer *et al.*, *ACS Catalysis*, 2017, **7**, 6207–6219.

35 G. Sun, J. An, H. Hu, C. Li, S. Zuo and H. Xia, *Catalysis Science & Technology*, 2019, **9**, 1238–1244.

36 A. Gupta, B. Boekfa, H. Sakurai, M. Ehara and U. D. Priyakumar, *The Journal of Physical Chemistry C*, 2016, **120**, 17454–17464.

37 P. Munnik, P. E. de Jongh and K. P. de Jong, *Chemical reviews*, 2015, **115**, 6687–6718.

38 Z. Yin, W. Zhou, Y. Gao, D. Ma, C. J. Kiely and X. Bao, *Chemistry–A European Journal*, 2012, **18**, 4887–4893.

39 M. V. Castegnaro, A. Gorgeski, B. Balke, M. d. C. M. Alves and J. Morais, *Nanoscale*, 2016, **8**, 641–647.

40 S. Steinhauer, J. Zhao, V. Singh, T. Pavloudis, J. Kioseoglou, K. Nordlund, F. Djurabekova, P. Grammatikopoulos and M. Sowwan, *Chemistry of Materials*, 2017, **29**, 6153–6160.

41 A. I. Frenkel, *Chemical Society Reviews*, 2012, **41**, 8163–8178.

42 A. Frenkel, *Zeitschrift für Kristallographie-Crystalline Materials*, 2007, **222**, 605–611.

43 Q. Yang, R. Hou and K. Sun, *Journal of Catalysis*, 2019, **374**, 12–23.

44 V. Litovchenko and A. Efremov, *Condensed Matter Physics*, 1999, 561–576.